



HAL
open science

Biodegradable Magnetic Molecularly Imprinted Anticancer Drug Carrier for the Targeted Delivery of Docetaxel

Zeeshan Ali, Muhammad Sajid, Suryyia Manzoor, Muhammad Mahboob Ahmad, Muhammad Imran Khan, Nouredine Elboughdiri, Muhammad Kashif, Abdallah Shanableh, Wajdi Rajhi, Wael Mersni, et al.

► **To cite this version:**

Zeeshan Ali, Muhammad Sajid, Suryyia Manzoor, Muhammad Mahboob Ahmad, Muhammad Imran Khan, et al.. Biodegradable Magnetic Molecularly Imprinted Anticancer Drug Carrier for the Targeted Delivery of Docetaxel. *ACS Omega*, 2022, 7 (32), pp.28516 - 28524. 10.1021/acsomega.2c03299 . hal-03762602

HAL Id: hal-03762602

<https://hal.science/hal-03762602>

Submitted on 28 Aug 2022

HAL is a multi-disciplinary open access archive for the deposit and dissemination of scientific research documents, whether they are published or not. The documents may come from teaching and research institutions in France or abroad, or from public or private research centers.

L'archive ouverte pluridisciplinaire **HAL**, est destinée au dépôt et à la diffusion de documents scientifiques de niveau recherche, publiés ou non, émanant des établissements d'enseignement et de recherche français ou étrangers, des laboratoires publics ou privés.

Biodegradable Magnetic Molecularly Imprinted Anticancer Drug Carrier for the Targeted Delivery of Docetaxel

Zeeshan Ali, Muhammad Sajid,* Suryyia Manzoor, Muhammad Mahboob Ahmad, Muhammad Imran Khan, Nouredine Elboughdiri,* Muhammad Kashif, Abdallah Shanableh, Wajdi Rajhi, Wael Mersni, Emin Bayraktar, and Sahbi Ben Salem



Cite This: *ACS Omega* 2022, 7, 28516–28524



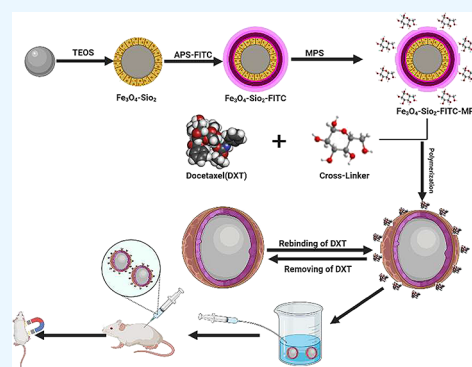
Read Online

ACCESS |

Metrics & More

Article Recommendations

ABSTRACT: Molecularly imprinted biodegradable polymers are receiving considerable attention in drug delivery due to their ability of targeted recognition and biocompatibility. This study reports the synthesis of a novel fluorescence-active magnetic molecularly imprinted drug carrier (MIDC) using a glucose-based biodegradable cross-linking agent for the delivery of anticancer drug docetaxel. The magnetic molecularly imprinted polymer (MMIP) was characterized through scanning electron microscopy (SEM), Fourier transform infrared spectroscopy (FTIR), X-ray diffraction spectroscopy, and vibrating sample magnetometry (VSM). The MMIP presented a magnetization value of 0.0059 emu g⁻¹ and binding capacity of 72 mg g⁻¹ with docetaxel. *In vitro* and *in vivo* studies were performed to observe the effectiveness of the MIDC for drug delivery. The cell viability assay suggested that the MMIP did not present toxic effects on healthy cells. The magnetic property of the MMIP allowed quick identification of the drug carrier at the target site by applying the external magnetic field to mice (after 20 min of loading) and taking X-ray images. The novel MMIP-based drug carrier could thus deliver the drug at the target site without affecting the healthy cells.



1. INTRODUCTION

Docetaxel (DTX) is an extract from a rare Pacific yew tree, *Taxus brevifolia*, and hence is classified as a plant alkaloid.¹ DTX possesses a side chain with tertbutyl carbamate ester and a carbon 10 hydroxy functional group. By binding and stabilizing tubulins, DTX prevents disintegration of the cell's physiological microtubules, resulting in G2/M cell cycle arrest and cell death. DTX also suppresses the anti-apoptotic expression of the Bcl2 gene and supports the expression of the p27 inhibition cell cycle.^{2–4} Its mechanism of action is effective against a wide variety of cancer tumors,⁴ including breast, ovarian, gastric, and prostate cancer.^{5–8}

Several drug carriers such as polymer drug conjugates,^{9,10} polymer protein conjugates,^{11,12} polymer micelles,^{13,14} polymeric nanoparticles,¹⁵ and gold nanoparticles^{16,17} have been used as carriers for a variety of drugs previously. Few drug nanocarriers such as galactosamine-D- α -tocopherol polyethylene glycol 1000 succinate-poly(lactide) (Gal-pD-TPGS-PLA/NPs) loaded with DTX have recently been reported with 55% release time in 14 days.¹⁸ Previous studies used chitosan-coated solid lipid nanoparticles (CS-SLNs) containing docetaxel for development and optimization. The high-pressure hot homogenization approach was used to create solid lipid nanoparticles (SLNs) with and without chitosan

coats, but the targeted selectivity and release of DTX were feeble.¹⁹ Monoolein cubic nanoparticles containing docetaxel were another carrier of DTX prepared by a top-down procedure through the homogenization technique with different amphiphile concentrations with a release rate of 24 h.²⁰ Therefore, further research on drug carriers focused on overcoming the side effects and fast release of DTX and improving its cancer effects is immensely required. Among various techniques, molecular imprinting polymerization is being deeply explored to synthesize biodegradable drug carriers. They possess a dominating characteristic of molecular recognition depending on the form, size, and interactions of the cavity produced by the template.^{21,22} Monomers usually form these polymers in the presence of a target molecule as the template and an excess of cross-linker.²³ MIPs are extremely efficient artificially manufactured receptors capable of rapid mass transfer and have high binding capacity.^{24,25} They display

Received: May 27, 2022

Accepted: July 22, 2022

Published: August 2, 2022



considerable extraction capabilities and can be modified to incorporate various properties like fluorescence activity, magnetic activity, etc. Magnetic MIPs have received prominent attention basically due to their outstanding properties such as magnetic susceptibility, small size, and high coercivity. They have also been considered suitable candidates in fields like bioengineering, catalysis, and bioseparation.²⁶ In molecularly imprinted polymer systems, recent magnetic separation techniques have received a lot of attention to facilitate separation by introducing an outside magnetic field.^{27,28} Such systems are capable of delivering loaded drugs at specific sites.²⁹ Various polymeric as well as sol–gel modifications can be performed to design magnetic imprinted drug carriers. One such example is $\text{Fe}_3\text{O}_4@\text{SiO}_2$ nanoparticle drug delivery systems.³⁰ The superparamagnetic core shell of iron silica is ideal for biomedical applications. They are protected and made acceptable for *in vivo* use by the surrounding polymeric layer. Iron nanoparticles are preferred over other forms of nanocarrier cancer therapy because their advantageous magnetic characteristics, higher chemical stability, minimal toxicity, and simplicity of surface modification are considered preferable to those of other nanocarriers for tumor-specific delivery of anticancer drugs.^{31,32} Additionally, iron nanoparticles of smaller sizes have several additional benefits, such as improved pharmacokinetics, better *in vivo* stability, and site-specific delivery of loaded cargo as well as increased internalization through the tumor vasculature (enhanced permeability and retention effect) and successful escape from the reticuloendothelial system (RES).³³ Furthermore, these synthetic or natural biodegradable materials in drug delivery systems enable them to be implanted in living organisms without further treatment.^{34,35} Other qualities such as stability in the 3D network, customizable drug release, elasticity, and flexibility with good mechanical characteristics are also beneficial in drug systems.³⁶ It has been shown that cross-linking polymers are usually stable and can protect their dimensions for longer periods. They offer a uniform biodegradability that may directly be changed by cross-linking density.³⁷ It has been observed that biologically degradable cross-linking polymers are among the most promising materials in targeted and regulated drug delivery.³⁸ Few papers are encountered in the literature regarding biodegradable molecularly imprinted polymers possessing magnetic characteristics and their applications in targeted drug delivery.^{39–41}

Hence, to further explore the unique traits of imprinted materials, we synthesized a novel fluorescent active magnetic molecularly imprinted polymer (MMIP) using glucose as the cross-linker. The synthesized MMIP was studied for its ability to deliver targeted drug docetaxel, an anticancer drug. Furthermore, the selection of glucose as the cross-linker describes this material as green, quick, and easy for rapid release of docetaxel at the target site.

2. MATERIALS AND METHODS

2.1. Materials and Reagents. Ferric chloride (FeCl_3) and ferrous sulfate heptahydrate ($\text{FeSO}_4 \cdot 7\text{H}_2\text{O}$), ammonia solution (33%), trisodium citrate ($\text{Na}_3\text{C}_6\text{H}_5\text{O}_7$, 99.0%), tetraethyl orthosilicate (TEOS, 99.9%), fluorescein-5-isothiocyanate (FITC), 3-aminopropyl trimethoxysilane vol (APTS), 3-trimethoxysilyl propyl methacrylate (MPS) 99.9–101%, toluene, triethylamine, methacryloyl chloride (99%), decane, 2,2'-azobis-2-methylpropionitrile (AIBN, 99.7%), sodium dodecyl sulfate (SDS), absolute ethanol (99.8%), acetone,

and acetonitrile (ACN) were purchased from Sigma Aldrich. Double distilled water was used for washing.

2.2. Synthesis of Magnetic Nanoparticles. The magnetic nanoparticles of Fe_3O_4 were synthesized by the coprecipitation method.⁴² 20 mmol of ferric chloride and 10 mmol of ferrous sulfate were mixed in 140 mL of water. The obtained solution was added into a two-neck round-bottom flask and purged under a N_2 atmosphere for 30 min. In this flask, 33 mL of 2 M ammonia solution was added dropwise under constant stirring till the precipitation of magnetic nanoparticles. After centrifugation, the brownish-black magnetic nanoparticles were washed with deionized water. An external magnetic field was applied to separate the nanoparticles. The isolated nanoparticles were then re-dispersed in 200 mL of water with 0.3 M trisodium citrate and heated at 70 °C for 2 h. After that, the nanoparticles were washed with acetone three times to remove the excess citrate and dried in a desiccator.

2.2.1. Modification of Magnetic Nanoparticles with Silica.

The citrate-modified magnetic nanoparticles were dispersed in 50 mL of water in an ultrasonic bath for 10 min. Next, 2 mL of dispersed nanoparticles was taken and diluted to 40 mL with distilled water. An ammonia solution (33%, 5 mL) and 140 mL of ethanol were added and mechanically stirred for 18 h. In the next step, tetraethyl orthosilicate (1 mL) was added dropwise to the mixture of dispersed nanoparticles and the reaction was allowed to proceed at room temperature for 16 h. The obtained material was then washed with distilled water and ethanol to remove any unreacted reagent. The silica-coated magnetic nanoparticles were dispersed in ethanol with the help of an ultrasonic tub.

2.2.2. Synthesis of FITC Magnetic Nanoparticles. The silica-coated fluorescent nanoparticles were synthesized according to the method by Huang et al.⁴³ A solution of fluorescence isothiocyanate FITC (0.04 g) in 10 mL of ethanol with APTS (0.22 mL) was mixed together and stirred for 18 h in the dark (solution A). Solution A was added to the flask containing silica-coated magnetic nanoparticles and mechanically agitated for 16 h. Fabricated FITC nanoparticles were obtained after drying at room temperature.

2.2.3. Modification with Methacryloxypropyl Trimethoxysilane. Finally, $\text{Fe}_3\text{O}_4@\text{SiO}_2@\text{FITC}$ nanoparticles were modified with methacryloxypropyl trimethoxysilane (MPS). For this purpose, 50 mL of toluene and 3 mL of MPS were mixed with $\text{Fe}_3\text{O}_4@\text{SiO}_2@\text{FITC}$ magnetic nanoparticles, and the reaction was performed at 70 °C with magnetic stirring for 15 h. After magnetic separation, these nanoparticles ($\text{Fe}_3\text{O}_4@\text{SiO}_2@\text{FITC}@\text{CH}_2=\text{CH}_2$) were modified with a double bond, washed with distilled water and ethanol, and stored in a desiccator at 40 °C.

2.2.4. Synthesis of the Cross-Linker. Glucose (1 mmol) and dry ACN were mixed in a Schlenk flask (10 mL). A few drops of $\text{N}(\text{C}_2\text{H}_5)_3$ (3 mmol) triethylamine and a solution of methacryloyl chloride (3 mmol) prepared in ACN were added into the Schlenk flask and stirred at 0 °C for 3 h. Finally, the unstable organics and extra methacryloyl chloride were rotary-evaporated, and the resultant solid was dried in a vacuum oven at 40 °C.

2.2.5. Fabrication of Molecularly Imprinted Polymer Nanoparticles. The MIP-coated Fe_3O_4 magnetic nanoparticles were synthesized using a microemulsion polymerization process. In the first step, to form a template monomer complex, cross-linker glucose (monomer) and docetaxel were

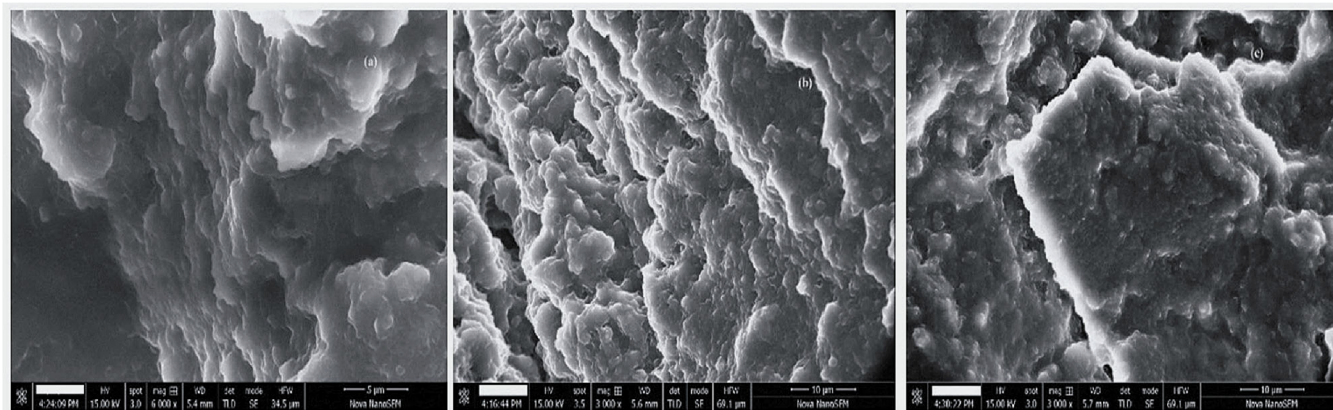


Figure 1. Scanning electron microscope images of Fe₃O₄ (a), silica-coated nanoparticles (b), and MMIPs (c).

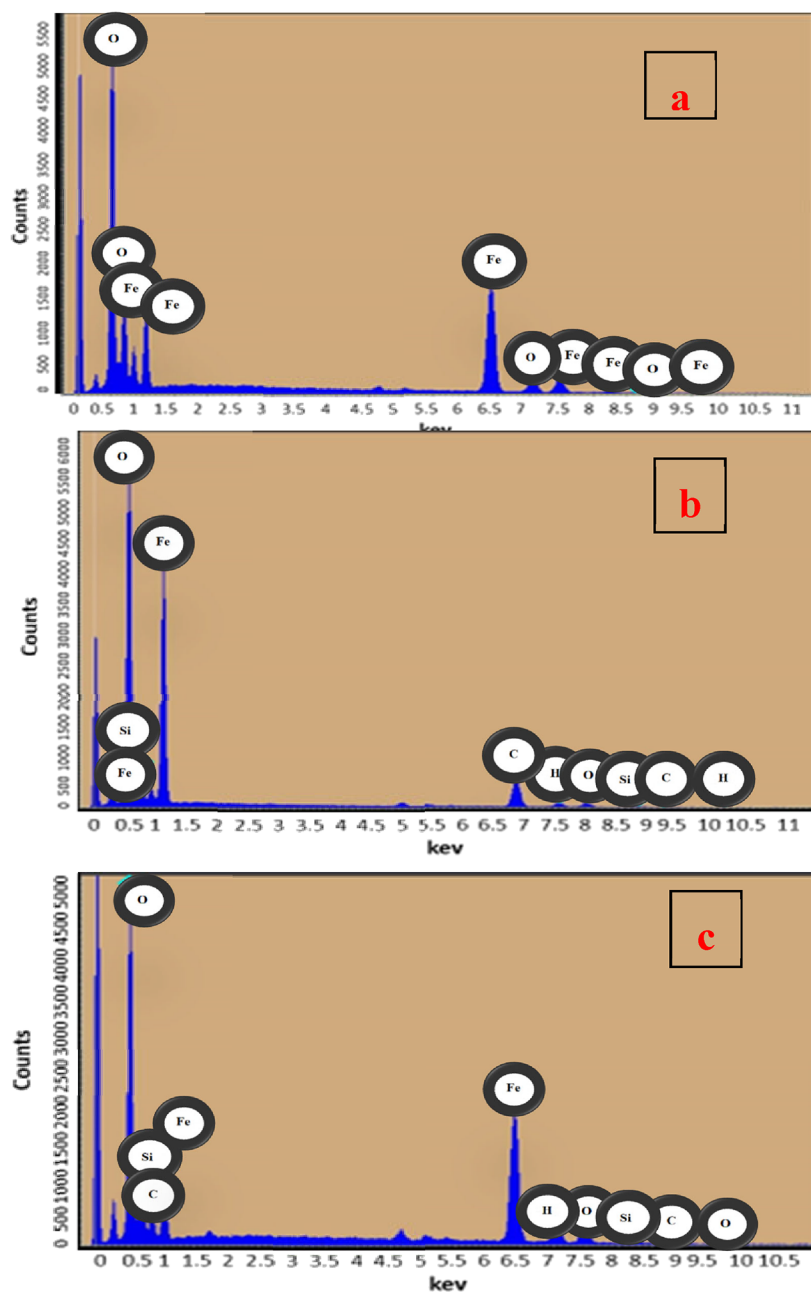


Figure 2. EDX diagrams of (a) Fe₃O₄, (b) silica-coated nanoparticles, and (c) the molecularly imprinted polymer.

dissolved in ACN/DMSO solution in a ratio of 5:1 (v/v). The solution was shaken for 5 h at room temperature. In the next step, 120 mg of modified magnetic nanoparticles and 60 mg of AIBN were added into ACN/DMSO solution and sonicated for 10 min. The reaction was continued under a N_2 atmosphere at 60 °C, and after 20 h, the fabricated imprinted polymer was collected using a strong external magnetic field, which was then washed with water and acetone.

Similarly, the non-imprinted polymer (NIP) was also synthesized using the same procedure in the absence of docetaxel. In the next step, both the drug-loaded MIP and NIP were administered orally to the mice with the help of a gavage. The mice's blood plasma was taken for drug detection and analyzed through HPLC.

2.3. Characterization of Nanomaterials. FTIR was used to study the functional groups present on the newly synthesized drug carrier. FTIR was performed using a Bruker Alpha II (USA) within the range 500–4000 cm^{-1} . The carbon, hydrogen, and oxygen contents were determined with a CHN analyzer (CHNO/S 2400 from PerkinElmer, USA). The phase angle of the materials was determined with X-ray Power diffraction (XRD-Powder D8 [Advance, Bruker Germany] with $Cu K\alpha$ radiation = 0.154 nm). The operational condition of XRD was a current of 30 mA and voltage of 40 kV for 2θ (20–80°). The particle size was determined using a scanning electron microscope (SEM) with an EDS and the E-Beam lithograph FEI Nova 450 NanoSEM. The magnetometry of magnetic nanoparticles, silica-coated magnetic nanoparticles, and MMIP nanoparticles was determined with VSM (Model 7407, Lakeshore, USA). The elemental composition was determined using EDS. In vitro drug location was performed with an X-ray analysis technique. The degradation of the MMIPs was performed at various pH levels. The dosage response of cell viability was studied with an MTT assay.

2.4. X-ray Analysis. For X-ray analysis, materials were made into tablets and placed on a gavage syringe. Two mice were taken and labeled with two dots at the tail for control and three dots at the tail for tablet containing medicine. An external magnetic field was used to attract materials. 30 min after administering the dose, X-ray images were taken. A magnetic field applied outside the body attracts the material, as evidenced by white spots on X-rays. Chloroform was used to make the mice comatose.

2.5. Blood Sample Analysis. The blood plasmas from blood samples of the mice were first separated through centrifugation. Then, the obtained plasmas were added to a mixture of acetic acid and methanol (8:2 v/v) in order to extract the drug. The extracted drug sample was analyzed through HPLC.

HPLC was performed using a Shimadzu LC-10 AT HPLC system (Japan) with a 266 nm UV detector and a reversed-phase column (ODS, C18 4.6 mm \times 250 mm, 5 μ waters USA). The mobile phase consisted of methanol:phosphate buffer (90:10 v/v), and the flow rate was adjusted to 0.5 mL min^{-1} .

3. RESULTS AND DISCUSSION

The synthetic scheme involves the MIP modified with fluorescence-active functional group FITC. Moreover, the magnetic properties were also introduced to the MIP through the incorporation of Fe_3O_4 nanoparticles. The main advantage of FITC is to locate or detect the drug inside the body (*in vivo* study) through fluorescence, and the purpose of glucose was to

serve as a biodegradable cross-linker replacing harmful cross-linkers such as tannic acid⁴⁴ commonly used in conventional synthesis.

3.1. Characterization. **3.1.1. Scanning Electron Microscopy.** Figure 1 shows the morphology of Fe_3O_4 NPs, Fe_3O_4 - SiO_2 NPs, and the MMIP nanoparticles. The Fe_3O_4 NPs were in minor accretion, according to published data of scanning electron microscopy,⁴⁵ with an average size of about 70 nm. Fe_3O_4 NPs were modified with TEOS (tetraethyl orthosilicate) to produce core-shell Fe_3O_4 - SiO_2 NPs with an average size range of 105 nm. The silica layer in the case of Fe_3O_4 - SiO_2 NPs was approximately 30 to 36 nm-thick. The shape of the MIP nanoparticles produced after the polymerization process remained spherical, and the diameter increased to 250 nm, indicating that this synthetic technique for MIP synthesis was successful. For measurement, two different nanoscales of 5 and 10 μm were used as given in Figure 1. The size of particles was confirmed by using software (Image J1.52v/ java 1.8.0_112 (64 bit)).

3.1.2. Elemental Detection Analysis. The elemental properties of materials were assessed through EDS analysis. The Fe, O, H, and Na peaks in Figure 2a indicate that iron nanoparticles were loaded with sodium citrate. The Fe, O, H, Na, S, and Si peaks in Figure 2b confirm the coating of silica. The peak at around 23 keV corresponds to S in the fluorescent layer, and the relatively higher amount of C in the MMIP pattern supports the production of a multicore-shell structure nanoparticle, as shown in Figure 2c.

3.1.3. Vibrating Sample Magnetometer. In Figure 3, magnetic nanoparticles (Fe_3O_4), silica-coated magnetic nano-

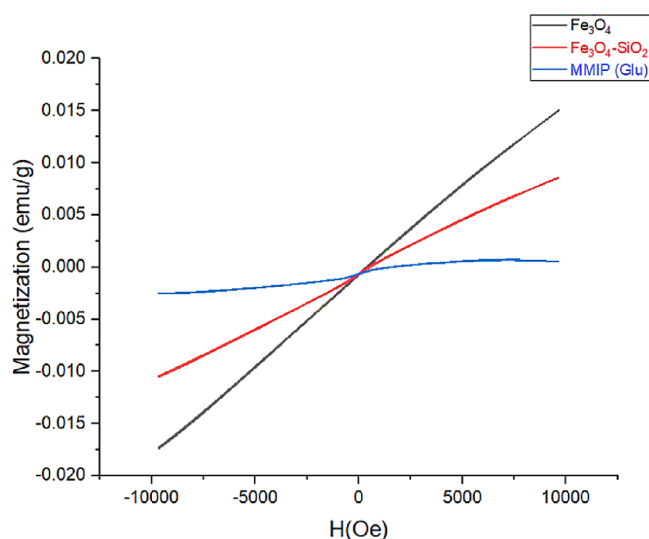


Figure 3. Vibrating sample magnetometer hysteresis loop of Fe_3O_4 , Fe_3O_4 - SiO_2 , and MMIPs.

particles (Fe_3O_4 - SiO_2), and the magnetic molecularly imprinted polymer (MMIP) loaded with docetaxel were tested using a vibrating sample magnetometer (VSM). Because of the pure magnetic material with no coatings or alterations, Fe_3O_4 nanoparticles have the highest capacity magnetization value. The magnetization of the second material is then reduced due to amalgamation with SiO_2 . After coating Fe_3O_4 - SiO_2 with cross-linkers and producing a polymer, the saturation magnetization decreased significantly. The magnetic characteristics of samples were thus altered to some extent after incorporating

various non-magnetic layers on Fe_3O_4 acting as the core, but they were still magnetic enough to respond to an external force (Table 1). A similar behavior was observed in previous studies.

Table 1. Magnetic Character of Fe_3O_4 , $\text{Fe}_3\text{O}_4\text{-SiO}_2$, and MMIP

material	magnetization (emu/g)
Fe_3O_4	0.01509
$\text{Fe}_3\text{O}_4\text{-SiO}_2$	0.00861
MMIP	0.000587

According to the trend of magnetization given in the literature for the synthesis of magnetic MIPs, the magnetization value reduced with the formation of the core shell and then decreased further after polymer formation.^{46,47}

3.1.4. Fourier Transform Infrared Spectroscopy. Fourier transform infrared spectroscopy (FTIR) is a technique for detecting various functional groups in organic and inorganic molecules. Figure 4a displays an Fe_3O_4 spectrograph with only

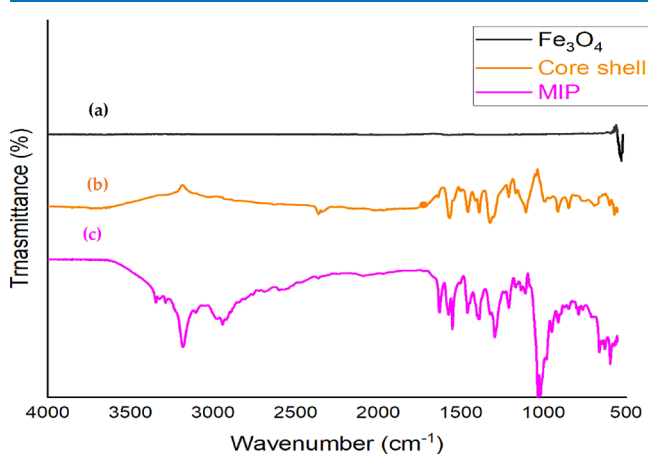


Figure 4. IR spectra of iron nanoparticles Fe_3O_4 (a), core-shell (b), and the magnetic molecularly imprinted polymer (c).

one conspicuous signal at 580 cm^{-1} , indicating that only Fe_3O_4 is present. In Figure 4b, a new strong peak appeared at 1085 cm^{-1} correlated to the Si–O–Si stretching vibration, and another peak appeared at around 800 cm^{-1} , which was referred to the Si–O stretching vibration and showed the successful encapsulation of SiO_2 onto the surface of Fe_3O_4 . In Figure 4c, the peaks at 3600 , 2990 , 2850 , 1730 , 1200 , 1090 , and 580 cm^{-1} represent many functional groups such as OH, C–H, C=O, C–C, and some bending frequencies of this spectrograph.

3.1.5. X-ray Diffraction Analysis. The crystalline structure of the drug carrier was determined by X-ray diffraction analysis. XRD was used to examine the structural characteristics of generated Fe_3O_4 , core shells, and MMIPs. Diffraction peaks in the 2θ region of 10° to 75° (30° , 35° , 43.5° , 53.6° , 56.0° , and 63°) with crystalline planes of (2 2 0), (3 1 1), (4 0 0), (4 2 2), (5 1 1), and (4 4 0), respectively (JCPDS NO. 19-0629), were in agreement with the typical spectrum of Fe_3O_4 NPs and identical to its core-shell, as shown in Figure 5. Broad peaks in the region of $2\theta = 12^\circ$ to 26° were observed in the XRD patterns of synthesized MMIPs, indicating the formation of an amorphous polymeric layer on the surface of Fe_3O_4 NPs. Furthermore, prominent reflection peaks in the range of $2\theta = 30^\circ$ to 75° were in agreement with the Fe_3O_4 pattern. The similarity of the patterns of Fe_3O_4 , core-shell, and MMIPs revealed that the crystallography of magnetic NPs was maintained during the creation of MMIPs on the surface of Fe_3O_4 . The intensity of signals or peaks decreases when we move from Fe_3O_4 to core-shell, and the intensity was further lowered from core-shell to the final product, which indicated the coating of silica and polymerization on Fe_3O_4 .

3.2. X-ray Analysis, MTT Assay, and Binding Capacity. The designed drug carrier possesses the benefit of quick identification through direct external application of a magnetic field. This was made possible by incorporating iron oxide nanoparticles in the drug carrier. Figure 6 confirms that the drug loaded with the carrier reached near the magnet after the mice were administered with the dose.

The dose-response data was used to measure the toxicity of the polymer toward healthy cells. Hence, the MTT (3-(4, 5-dimethylthiazol-2-yl)-2,5-diphenyl-2H-tetrazolium bromide)

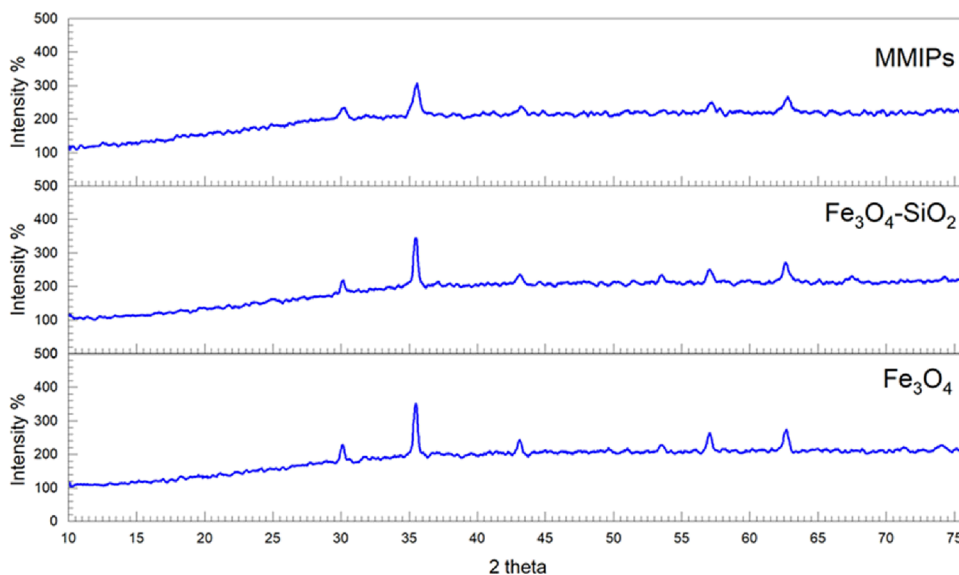


Figure 5. XRD graph of Fe_3O_4 , silica-coated nanoparticles, and the magnetic molecularly imprinted polymer.

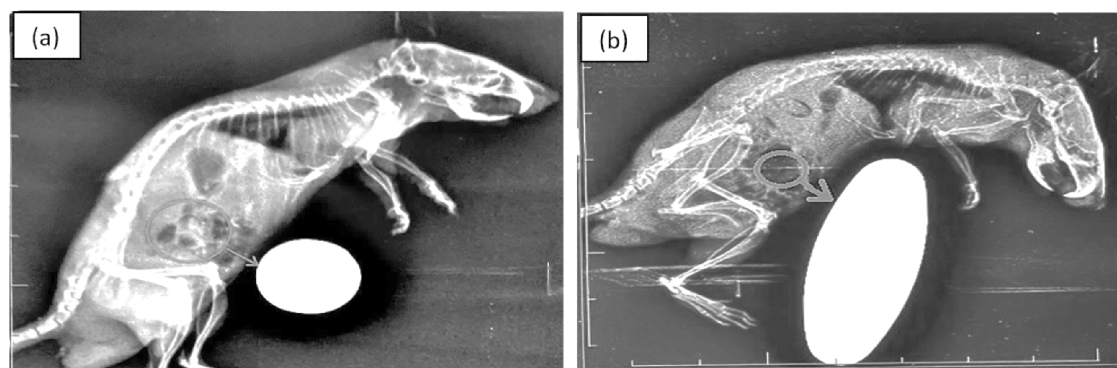


Figure 6. X-ray analysis image of mice loaded with (without drug) a tablet dose (a) and a MIP tablet dose (b).

assay was performed describing the percentage of living cells. The cell viability of the polymer was measured against non-cancerous cell lines (HepG2) and is given in Figure 7. This

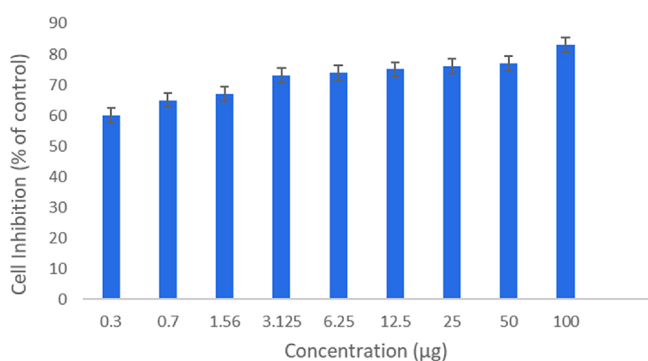


Figure 7. Effect of concentration of MIDC on cell viability.

data showed that by increasing the concentration of polymer (MIDC), the percentage of living cells increased, proving that the polymer is non-toxic to healthy cells. When the concentration was changed from 0.3 to 100 µg, the percentage of living cells increased from 60% to 83% and these values were calculated after 72 h.

The amount of docetaxel bound to the MMIP was calculated using eq 1.

$$q = \frac{(C_0 - C_f)}{m} \times v \quad (1)$$

where q (mg g^{-1}), C_0 (mg mL^{-1}), C_f (mg L^{-1}), V (L), and m (g) are the adsorption capacity, initial and final concentrations of DTX, sample volume, and mass of MMIP, respectively. The binding capacity was thus found to be 72 mg g^{-1} .

3.3. Blood Sample Analysis. The drug released into the blood stream was investigated by analyzing the blood plasmas collected from the mice that were orally administered with the MMIP and MNIP. In Figure 8a, the primary standard drug was used as a reference and its peak appeared after 4 min of sample loading. In the case of the MNIP, the peak of the docetaxel did not appear in the HPLC chromatogram (Figure 8b), while the relevant peak of the drug was observed at a retention time of 4 min in the chromatogram obtained by using the MMIP (Figure 8c). This confirms the drug release from the MIP into the blood at the targeted site. Figure 8d shows the overlap of all the three chromatograms. Three types of chromatograms of the sample, standard, and MMIPs without the drug were taken

for such analysis. From these values, the percentage recovery was calculated by applying the following equation

$$\text{percentage recovery} = \frac{C(\text{found}) - C(\text{real})}{C(\text{added})} \times 100$$

C_{found} and C_{real} were calculated from their respective peak areas, and C_{added} is the spiked amount. The percentage recovery of 96% ($n = 9$) was thus obtained.

The expected mechanism of drug loading and release involves the formation of hydrogen bonds between the drug and cross-linker. Docetaxel contains various functional groups such as amino, hydroxyl, and carbonyl that can interact with glucose (cross-linker). These interactions are possibly reversible in aqueous medium; therefore, it was anticipated that the drug would probably release in the stomach due to its favorable environment.

3.4. Degradation Test. Studying the material's self-degradation ability provides the most vital information for its selection in biomedical uses because its presence in the body for an extended period may be detrimental. At pH = 3, which is close to the stomach environment, and pH = 7.35, which is close to the physical state, the degradation of the MMIP was investigated (Table 2). The deterioration rate at pH = 3 (stomach environment) was faster than at pH 7.35, according to the data (Figure 9). Furthermore, the data show that material breakdown was faster in acidic and basic environments than in the body's natural pH of 7.4. The discovered results are connected to the glucose-based cross-linker in the molecularly imprinted polymer structure.

3.5. Comparative Study. Though docetaxel is among one of the commonly employed anticancer drugs, its targeted drug delivery through MMIP has not been studied previously. The MMIP synthesized in this work for this purpose presented a binding capacity of 72 mg g^{-1} . This value was compared with other drugs that have also been studied for the targeted delivery using MIPs as carriers. It is eminent to mention here that these MIPs were obtained through different synthetic schemes. Table 3 clearly depicts that the MMIP reported in this study presented a q_e value comparable to others and hence can successfully be selected as a potential drug carrier for the targeted delivery.

4. CONCLUSIONS

This study was based on the synthesis of fluorescence-active MMIP using a glucose cross-linker to create docetaxel-loaded unique multicore-shell structure nanocarriers. The final product was in the nano range, which can facilitate its in

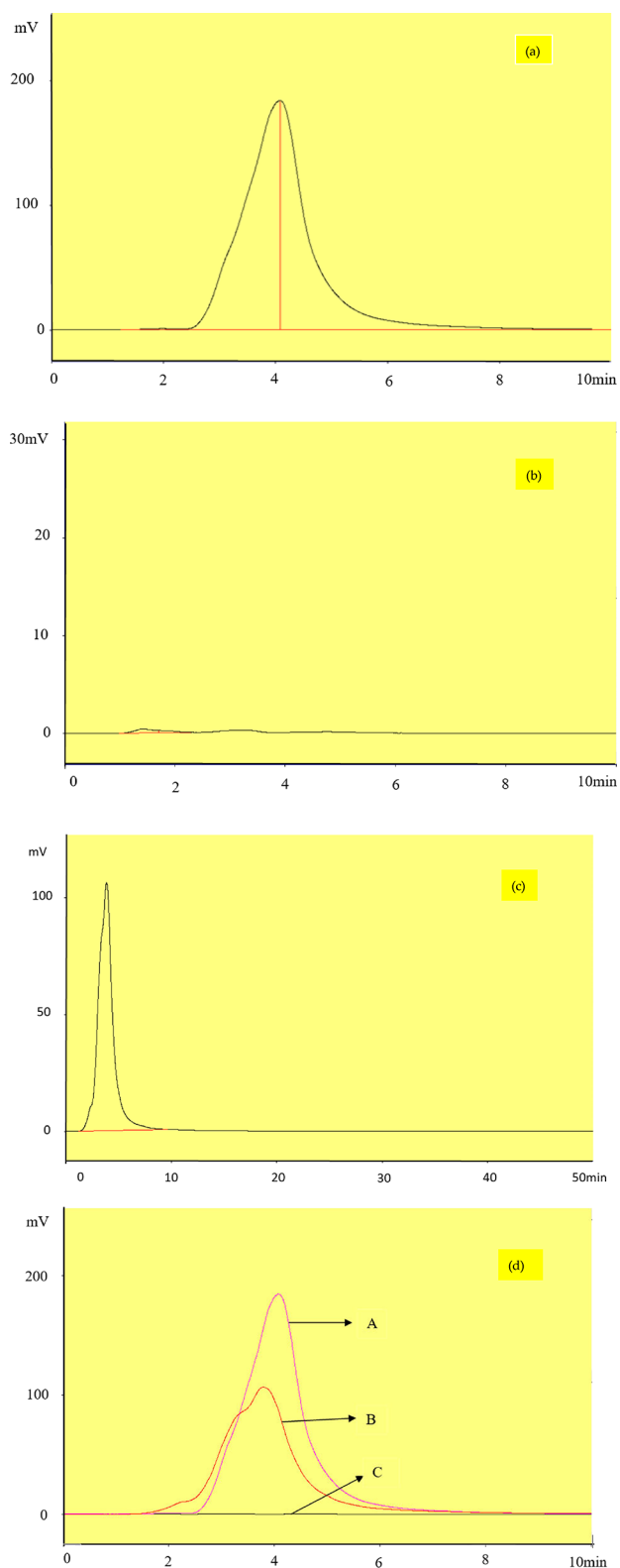


Figure 8. Chromatogram of 100 mg L⁻¹ mobile phase (90–10 methanol/phosphate buffer (v/v %), flow rate of 0.5 mL min⁻¹: (a) standard docetaxel, (b) blood plasma loaded with the MNIP, (c) and blood plasma loaded with MMIPs; (d) overlay of three chromatograms (a–c).

vivo movement. The MMIP exhibited an acceptable magnetic property for its detection through an external magnetic field. Moreover, due to the need for non-toxic materials in medical

Table 2. Values of Percentage Remaining Weight against Time at Different pH Levels

sr. no.	soaking time (day)	weight remaining (%) at pH 3	weight remaining (%) at pH 7.35
1	1	100	100
2	2	93	96
3	3	91	93
4	4	88	92
5	5	87	91
6	6	86	90
7	7	84	88
8	8	83	88
9	9	82	87
10	10	82	86

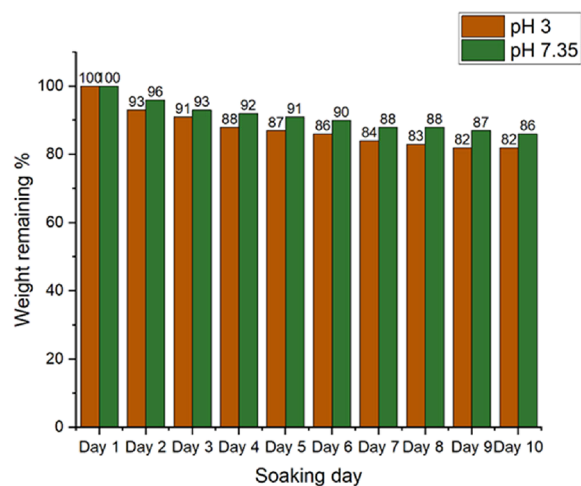


Figure 9. Degradation of the magnetic molecularly imprinted polymer at neutral and acidic pH.

Table 3. Comparison of the Current Study with the Previously Reported Work

reference	template	qMIP (mg g ⁻¹)
48	bisphenol A	0.129
49	diphenyl amine A	31
47	5-fluorouracil	45
50	curcumin	77
our work	docetaxel	72

applications, several studies were developed to prove the biocompatibility of such materials. The MTT viability assay showed the MMIP's non-toxic nature. In vitro drug release in simulated stomach fluid showed a fast release profile. A q_e value of 72 mg g⁻¹ describes its ability to load a considerable amount of drug. Overall, the findings show that the described MMIP can be exploited as a substantial device in drug delivery applications for malignant tissue treatment due to its exceptional features and diversified performances.

■ AUTHOR INFORMATION

Corresponding Authors

Muhammad Sajid – Institute of Chemical Sciences, Bahauddin Zakariya University, Multan 60000, Pakistan;

Phone: 00923040801998; Email: msajidkang@gmail.com

Noureddine Elboughdiri – Chemical Engineering Process Department, National School of Engineers Gabes, University of Gabes, Gabes 6011, Tunisia; orcid.org/0000-0003-

2923-3062; Phone: 00966549571015;

Email: ghilaninouri@yahoo.fr

Authors

Zeeshan Ali – Institute of Chemical Sciences, Bahauddin Zakariya University, Multan 60000, Pakistan

Suryya Manzoor – Institute of Chemical Sciences, Bahauddin Zakariya University, Multan 60000, Pakistan

Muhammad Mahboob Ahmad – Institute of Chemical Sciences, Bahauddin Zakariya University, Multan 60000, Pakistan

Muhammad Imran Khan – Research Institute of Sciences and Engineering (RISE), University of Sharjah, Sharjah 27272, United Arab Emirates

Muhammad Kashif – Department of Chemistry, Emerson University, Multan 60000, Pakistan

Abdallah Shanableh – Research Institute of Sciences and Engineering (RISE), University of Sharjah, Sharjah 27272, United Arab Emirates

Wajdi Rajhi – Mechanical Engineering Department, College of Engineering, University of Ha'il, Ha'il 81441, Saudi Arabia

Wael Mersni – National School of Engineers of Tunis, University of Tunis El Manar, Tunis 1068, Tunisia

Emin Bayraktar – School of Mechanical and Manufacturing Engineering, ISAE-SUPMECA Institute of Mechanics of Paris, Saint-Ouen 93400, France

Sahbi Ben Salem – National School of Engineers of Tunis, University of Tunis El Manar, Tunis 1068, Tunisia

Complete contact information is available at:

<https://pubs.acs.org/10.1021/acsomega.2c03299>

Notes

The authors declare no competing financial interest.

All the data in this study is provided in the manuscript.

ACKNOWLEDGMENTS

This research has been funded by the Research Deanship of University of Ha'il, Saudi Arabia, through the Project RG-20 122. The authors are grateful to higher Education Commission (HEC), and the Department of Pharmacy Bahauddin Zakariya University Multan, Pakistan for providing the lab facility to conduct this research work.

REFERENCES

- (1) Clarke, S. J.; Rivory, L. P. Clinical pharmacokinetics of docetaxel. *Clin. Pharmacokinet.* **1999**, *36*, 99–114.
- (2) Snyder, J. P.; Nettles, J. H.; Cornett, B.; Downing, K. H.; Nogales, E. The binding conformation of Taxol in β -tubulin: a model based on electron crystallographic density. *Proc. Natl. Acad. Sci. U. S. A.* **2001**, *98*, 5312–5316.
- (3) Yvon, A. M. C.; Wadsworth, P.; Jordan, M. A. Taxol suppresses dynamics of individual microtubules in living human tumor cells. *Mol. Biol. Cell* **1999**, *10*, 947–959.
- (4) Van Poppel, H. Recent docetaxel studies establish a new standard of care in hormone refractory prostate cancer. *Can. Urol.* **2005**, *12*, 81–85.
- (5) Chevallier, B.; Fumoleau, P.; Kerbrat, P.; Dieras, V.; Roche, H.; Krakowski, I.; Azli, N.; Bayssas, M.; Lentz, M. A.; Van Glabbeke, M. Docetaxel is a major cytotoxic drug for the treatment of advanced breast cancer: a phase II trial of the Clinical Screening Cooperative Group of the European Organization for Research and Treatment of Cancer. *J. Clin. Oncol.* **1995**, *13*, 314–322.
- (6) Fossella, F. V.; Lee, J. S.; Shin, D. M.; Calayag, M.; Huber, M.; Perez-Soler, R.; Murphy, W. K.; Lippman, S.; Benner, S.; Glisson, B.

Phase II study of docetaxel for advanced or metastatic platinum-refractory non-small-cell lung cancer. *J. Clin. Oncol.* **1995**, *13*, 645–651.

(7) Kaye, S. B.; Piccart, M.; Aapro, M.; Francis, P.; Kavanagh, J. Phase II trials of docetaxel (Taxotere®) in advanced ovarian cancer—an updated overview. *Eur. J. Cancer* **1997**, *33*, 2167–2170.

(8) Mavroudis, D.; Kourousis, C.; Androulakis, N.; Kalbakis, K.; Agelaki, S.; Kakolyris, S.; Souglakos, J.; Sarra, E.; Vardakis, N.; Hatzidaki, D.; Sarmonis, G.; Georgoulis, V. Frontline treatment of advanced gastric cancer with docetaxel and granulocyte colony-stimulating factor (G-CSF): a phase II trial. *Am. J. Clin. Oncol.* **2000**, *23*, 341–344.

(9) Ekladius, I.; Colson, Y. L.; Grinstaff, M. W. Polymer–drug conjugate therapeutics: advances, insights and prospects. *Nat. Rev. Drug Discovery* **2019**, *18*, 273–294.

(10) Shariatina, Z. Big family of nano- and microscale drug delivery systems ranging from inorganic materials to polymeric and stimuli-responsive carriers as well as drug-conjugates. *J. Drug Delivery Sci. Technol.* **2021**, *66*, 102790.

(11) Trzebiecka, B.; Szweda, R.; Kosowski, D.; Szweda, D.; Otulakowski, L.; Haladjova, E.; Dworak, A. Thermoresponsive polymer-peptide/protein conjugates. *Prog. Polym. Sci.* **2017**, *68*, 35–76.

(12) Stevens, C. A.; Kaur, K.; Klok, H. A. Self-assembly of protein-polymer conjugates for drug delivery. *Adv. Drug Delivery Rev.* **2021**, *174*, 447–460.

(13) Yokoyama, M. Polymeric micelles as drug carriers: their lights and shadows. *J. Drug Targeting* **2014**, *22*, 576–583.

(14) Shi, L.; Lu, S.; Sun, T.; Xi, G.; Chen, Z.; Xu, K.; Zhao, X.; Shen, M.; Jia, T.; Zhao, X. Robust fluorescent amphiphilic polymer micelle for drug carrier application. *New J. Chem.* **2021**, *45*, 9409–9415.

(15) Zhang, W. J.; Hong, C. Y.; Pan, C. Y. Polymerization-induced self-assembly of functionalized block copolymer nanoparticles and their application in drug delivery. *Macromol. Rapid Commun.* **2019**, *40*, 1800279.

(16) Siddique, S.; Chow, J. C. L. Gold nanoparticles for drug delivery and cancer therapy. *Appl. Sci.* **2020**, *10*, 3824.

(17) He, J. S.; Liu, S. J.; Zhang, Y. R.; Chu, X. D.; Lin, Z. B.; Zhao, Z.; Qiu, S. H.; Guo, Y. G.; Ding, H.; Pan, Y. L.; Pan, J. H. The application of and strategy for gold nanoparticles in cancer immunotherapy. *Front. Pharmacol.* **2021**, *12*, 687399.

(18) Zhu, D.; Tao, W.; Zhang, H.; Liu, G.; Wang, T.; Zhang, L.; Zeng, X.; Mei, L. Docetaxel (DTX)-loaded polydopamine-modified TPGS-PLA nanoparticles as a targeted drug delivery system for the treatment of liver cancer. *Acta Biomater.* **2016**, *30*, 144–154.

(19) Dawoud, M. Chitosan coated solid lipid nanoparticles as promising carriers for docetaxel. *J. Drug Delivery Sci. Technol.* **2021**, *62*, 102409.

(20) Dawoud, M.; Abourehab, M. A. S.; Abdou, R. Monoolein cubic nanoparticles as novel carriers for docetaxel. *J. Drug Delivery Sci. Technol.* **2020**, *56*, 101501.

(21) Ndunda, E. N. Molecularly imprinted polymers—a closer look at the control polymer used in determining the imprinting effect: a mini review. *J. Mol. Recognit.* **2020**, *33*, No. e2855.

(22) Vasapollo, G.; Sole, R. D.; Mergola, L.; Lazzoi, M. R.; Scardino, A.; Scorrano, S.; Mele, G. Molecularly imprinted polymers: present and future prospective. *Int. J. Mol. Sci.* **2011**, *12*, 5908–5945.

(23) Köse, K.; Kehribar, D. Y.; Uzun, L. Molecularly imprinted polymers in toxicology: A literature survey for the last 5 years. *Environ. Sci. Pollut. Res.* **2021**, *28*, 35437–35471.

(24) Ostovan, A.; Ghaedi, M.; Arabi, M.; Asfaram, A. Hollow porous molecularly imprinted polymer for highly selective clean-up followed by influential preconcentration of ultra-trace glibenclamide from biofluid. *J. Chromatogr. A.* **2017**, *1520*, 65–74.

(25) Dong, C.; Shi, H.; Han, Y.; Yang, Y.; Wang, R.; Men, J. Molecularly imprinted polymers by the surface imprinting technique. *Eur. Polym. J.* **2021**, *145*, 110231.

- (26) Gopi, S.; Amalraj, A.; Sukumaran, N. P.; Haponiuk, J. T.; Thomas, S. Biopolymers and their composites for drug delivery: a brief review. *Macromol. Symp.* **2018**, *380*, 1800114.
- (27) Ansari, S. Application of magnetic molecularly imprinted polymer as a versatile and highly selective tool in food and environmental analysis: Recent developments and trends. *Trends Anal. Chem.* **2017**, *90*, 89–106.
- (28) Ansari, S.; Karimi, M. Recent configurations and progressive uses of magnetic molecularly imprinted polymers for drug analysis. *Talanta* **2017**, *167*, 470–485.
- (29) Zhao, Y.; Feng, Z.; Li, S.; Lu, Y.; Hu, Y.; Fan, H.; Zhai, X. Preparation of Magnetic Molecularly Imprinted Polymers for Selective Recognition and Determination of Clenbuterol in Pork Samples. *J. Chem.* **2020**, 8820262.
- (30) Yang, C.; Li, Y.; Yang, Y.; Chen, Z. Overview of strategies to improve therapy against tumors using natural killer cell. *J. Immunol. Res.* **2020**, 8459496.
- (31) Esmailpour, M.; Zahmatkesh, S. Chemistry, Palladium nanoparticles immobilized on EDTA-modified Fe₃O₄@ SiO₂: a highly stable and efficient magnetically recoverable catalyst for the Heck–Mizoroki coupling reactions. *Inorg. Nano-Met. Chem.* **2019**, *49*, 267–276.
- (32) Hashemi-Moghaddam, H.; Kazemi-Bagsangani, S.; Jamili, M.; Zavareh, S. Evaluation of magnetic nanoparticles coated by 5-fluorouracil imprinted polymer for controlled drug delivery in mouse breast cancer model. *Int. J. Pharm. (Amsterdam, Neth.)* **2016**, *497*, 228–238.
- (33) Wahajuddin; Arora, S. Superparamagnetic iron oxide nanoparticles: magnetic nanoplatforms as drug carriers. *Int. J. Nanomed.* **2012**, *7*, 3445.
- (34) Alvarez-Lorenzo, C.; Concheiro, A. Smart drug delivery systems: from fundamentals to the clinic. *Chem. Commun.* **2014**, *50*, 7743–7765.
- (35) Sung, Y. K.; Kim, S. W. Recent advances in polymeric drug delivery systems. *Biomater. Res.* **2020**, *24*, 1–12.
- (36) Ogay, V.; Mun, E. A.; Kudaibergen, G.; Baidarbekov, M.; Kassymbek, K.; Zharkinbekov, Z.; Saparov, A. Progress and prospects of polymer-based drug delivery systems for bone tissue regeneration. *Polymer* **2020**, *12*, 2881.
- (37) Gong, M.; Xiao, J.; Li, H.; Hai, L.; Yang, K.; Li, J.; Wang, Z.; Deng, L.; He, D. Magnetically retained and glucose-fueled hydroxyl radical nanogenerators for H₂O₂-self-supplying chemodynamic therapy of wound infections. *Mater. Sci. Eng., C* **2021**, *131*, 112522.
- (38) Qin, Y. T.; Feng, Y. S.; Ma, Y. J.; He, X. W.; Li, W. Y.; Zhang, Y. K. Tumor-sensitive biodegradable nanoparticles of molecularly imprinted polymer-stabilized fluorescent zeolitic imidazolate framework-8 for targeted imaging and drug delivery. *ACS Appl. Mater. Interfaces* **2020**, *12*, 24585–24598.
- (39) He, S.; Zhang, L.; Bai, S.; Yang, H.; Cui, Z.; Zhang, X.; Li, Y. Advances of molecularly imprinted polymers (MIP) and the application in drug delivery. *Eur. Polym. J.* **2021**, *143*, 110179.
- (40) Shevchenko, K. G.; Garkushina, I. S.; Canfarotta, F.; Piletsky, S. A.; Barlev, N. A. Nano-molecularly imprinted polymers (nanoMIPs) as a novel approach to targeted drug delivery in nanomedicine. *RSC Adv.* **2022**, *12*, 3957–3968.
- (41) Liu, R.; Poma, A. Advances in molecularly imprinted polymers as drug delivery systems. *Molecules* **2021**, *26*, 3589.
- (42) Yang, D.; Hu, J.; Fu, S. Controlled synthesis of magnetite–silica nanocomposites via a seeded sol–gel approach. *J. Phys. Chem. C* **2009**, *113*, 7646–7651.
- (43) Huang, J.; Liu, H.; Men, H.; Zhai, Y.; Xi, Q.; Zhang, Z.; Zhang, J.; Yin, Z.; Li, L. Molecularly imprinted polymer coating with fluorescence on magnetic particle. *Macromol. Res.* **2013**, *21*, 1021–1028.
- (44) Chung, K. T.; Wong, T. Y.; Wei, C. I.; Huang, Y. W.; Lin, Y. Tannins and human health: a review. *Crit. Rev. Food Sci. Nutr.* **1998**, *38*, 421–464.
- (45) Dong, H.; Zhao, F.; He, Q.; Xie, Y.; Zeng, Y.; Zhang, L.; Tang, L.; Zeng, G. Physicochemical transformation of carboxymethyl cellulose-coated zero-valent iron nanoparticles (nZVI) in simulated groundwater under anaerobic conditions. *Sep. Purif. Technol.* **2017**, *175*, 376–383.
- (46) Cheng, Y.; Nie, J.; Li, J.; Liu, H.; Yan, Z.; Kuang, L. Synthesis and characterization of core–shell magnetic molecularly imprinted polymers for selective recognition and determination of quercetin in apple samples. *Food Chem.* **2019**, *287*, 100–106.
- (47) Asadi, E.; Abdouss, M.; Leblanc, R. M.; Ezzati, N.; Wilson, J. N.; Azodi-Deilami, S. In vitro/in vivo study of novel anti-cancer, biodegradable cross-linked tannic acid for fabrication of 5-fluorouracil-targeting drug delivery nano-device based on a molecular imprinted polymer. *RSC Adv.* **2016**, *6*, 37308–37318.
- (48) Zhang, Z.; Chen, X.; Rao, W.; Chen, H.; Cai, R. Synthesis and properties of magnetic molecularly imprinted polymers based on multiwalled carbon nanotubes for magnetic extraction of bisphenol A from water. *J. Chromatogr., B* **2014**, *965*, 190–196.
- (49) Hande, P. E.; Samui, A. B.; Kulkarni, P. S. A molecularly imprinted polymer with flash column chromatography for the selective and continuous extraction of diphenyl amine. *RSC Adv.* **2015**, *5*, 73434–73443.
- (50) Sedghi, R.; Yassari, M.; Heidari, B. Thermo-responsive molecularly imprinted polymer containing magnetic nanoparticles: Synthesis, characterization and adsorption properties for curcumin. *Colloids Surf., B* **2018**, *162*, 154–162.

Recommended by ACS

Epitope Molecularly Imprinted Polymer Nanoparticles for Chemo-/Photodynamic Synergistic Cancer Therapy Guided by Targeted Fluorescence Imaging

Hui Peng, Yu-Kui Zhang, *et al.*

FEBRUARY 26, 2020
ACS APPLIED MATERIALS & INTERFACES

READ 

Hypoxia-Responsive Polypeptide Nanoparticles Loaded with Doxorubicin for Breast Cancer Therapy

Peng Zhang, Chunsheng Xiao, *et al.*

MARCH 10, 2020
ACS BIOMATERIALS SCIENCE & ENGINEERING

READ 

Size-Transformable Hyaluronan Stacked Self-Assembling Peptide Nanoparticles for Improved Transcellular Tumor Penetration and Photo-Chemo...

Zhaoqing Cong, Yong-Hong Liao, *et al.*

FEBRUARY 05, 2020
ACS NANO

READ 

Surface Charge Switchable Polymer/DNA Nanoparticles Responsive to Tumor Extracellular pH for Tumor-Triggered Enhanced Gene Delivery

Ying Jie Ooi, Jun Li, *et al.*

JANUARY 16, 2020
BIOMACROMOLECULES

READ 

Get More Suggestions >